Electric Power Systems Research 178 (2020) 106023

Contents lists available at ScienceDirect

Electric Power Systems Research

journal homepage: www.elsevier.com/locate/epsr

A new method for discrimination of internal fault from other transient states in power transformer using Clarke's transform and modified hyperbolic S-transform

Abdolreza Behvandi*, Seyed Ghodratollah Seifossadat, Alireza Saffarian

Department of Electrical Engineering, Faculty of Engineering, Shahid Chamran University of Ahvaz, Ahvaz, Iran

ARTICLE INFO

Keywords:
Differential protection
Modified hyperbolic Stockwell transform
Internal fault
Ultra-saturation
Over-excitation

ABSTRACT

In this paper, a new method is proposed for discriminating internal faults from other abnormal conditions in power transformers such as inrush currents, external faults, over-excitation, and ultra-saturation. Since the differential current signals are non-stationary, a powerful tool such as S-transform is needed for their time-frequency analysis. In this study, some important characteristics are extracted using the Clark's transform and modified hyperbolic S-transform according to which different conditions are distinguished and classified. These features include energy contour of first level, variance index, standard deviation of second harmonic component, and a special criterion. In this paper, all possible transient conditions and the effects of the saturation of current transformers are considered. Various simulations for different operating conditions of transformer are performed via PSCAD/EMTDC software. Also, the entire process of modified hyperbolic S-transform and the proposed algorithm are done in MATLAB software. Simulation results show that the proposed algorithm can be reliably used for the identification and classification of different faults in transformers.

1. Introduction

Since power transformers transmit large amounts of power in electrical power systems, they are among the most important components in power systems. Almost 10% of power system faults occur in transformers, and 70% of these faults are caused by short circuit in transformer windings [1]. Therefore, faults in transformer are usually considered an important disturbance in transmission networks [2].

The outage rate of a power transformer depends on several factors such as the operating condition of the power transformer, the periodical maintenance, the power transformer's lifetime and the mal-operation of protection [3]. Abnormal conditions that lead to relay mal-operation include internal faults, inrush currents caused by energizing transformers, external faults, over-excitation and ultra-saturation. Accurately discrimination of internal faults from other conditions has long been recognized as a challenge in power transformer protection [4]. Thus, using a suitable protection system is necessary.

One of the important reasons for mal-operation in transformer protection is the magnetizing inrush current that is produced during transformer energizing. The inrush current contains a considerable second harmonic component [5]. Thus, the harmonic restraint method as one of the first methods of recognition of inrush current uses the ratio of differential current second harmonic and fundamental frequency. In Ref. [6], some algorithms based on second harmonic are suggested to distinguish between the inrush current from internal faults. This method is based on the fact that in inrush current conditions, second harmonic content is greater compared to internal fault conditions. On the other hand, CT saturation or the presence of a shunt capacitor or the distributive capacitance in a long extra high-voltage (EHV) transmission line to which the transformer may be connected increases the second harmonic in internal faults [7]. The disadvantage of this method is that it is possible for whatever reason, that the second harmonic content in internal fault will be a considerable amount as well. Moreover, by using more developed materials in manufacturing modern transformer cores, the second harmonic component in magnetizing inrush currents tends to be relatively small [8,9]. To overcome such a problem, a novel approach is presented in Ref. [10]. Conventional inrush current blocking methods including the second harmonic and gap detection criteria are combined. Thus, the proposed strategy has the potential for industrial implementation.

Some modern methods based on Artificial Neural Network (ANN) and optimization algorithm [4], Fuzzy logic [11] and Hidden Markov model [12] have been presented. The limitation of the methods based on learning is that a large size of data is needed for the training process.

* Corresponding author.
E-mail address: a-behvandi@phdstu.scu.ac.ir (A. Behvandi).

https://doi.org/10.1016/j.epsr.2019.106023
Received 12 November 2018; Received in revised form 3 April 2019; Accepted 1 September 2019
Available online 12 September 2019
0378-7796/

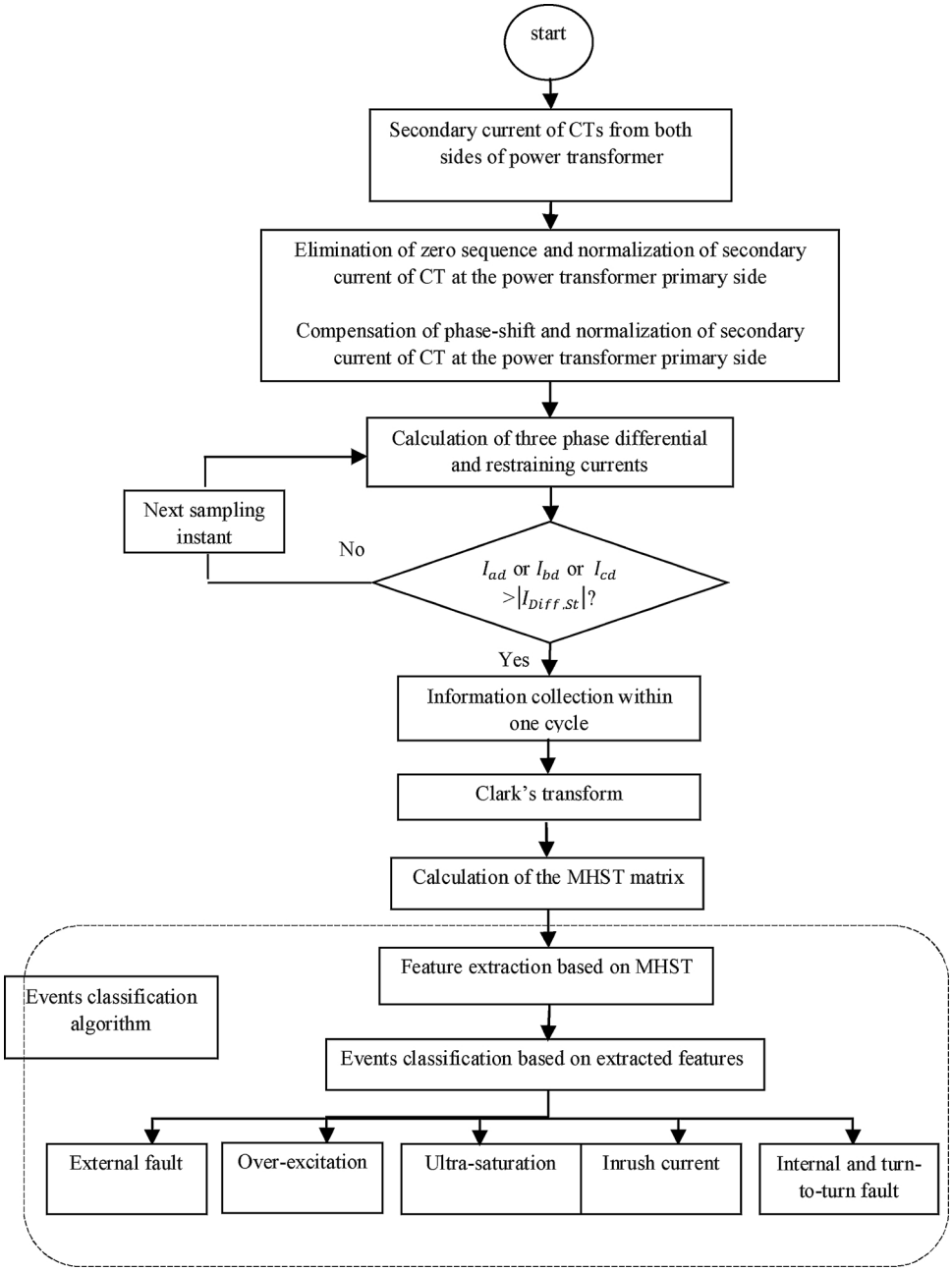

Fig. 1. The flowchart of the proposed method for transformer differential protection scheme.

In addition, the suitable structure in these methods is chosen by trial and error, and as a result, the learning process requires a long time.

A wavelet transform (WT) is a powerful tool in signal processing. Therefore, in Refs. [13–18], methods based on wavelet transform for the protection of transformers are presented. The method presented in Ref. [13] uses the time difference between disturbance and CT saturation moments in order to recognize the faults. In Ref. [14] a detailed wave wave-form of wavelet is applied to detect the transient conditions. In Ref. [15], a new method based on wavelet packet is implemented to discriminate inrush currents from internal faults. Also, in some methods, hybrid models of wavelet transform and support vector machine [16] in addition to coherence coefficient concept [17] are used.

Because of immunity against noise, S-transform is used in power system studies [19,20] and transformer protection [21]. Due to low energy concentration of an S-transform in the time- frequency domain, applying hyperbolic window instead of Gaussian window is suggested [22,23]. This method is known as the hyperbolic S transform. In Ref. [24], time- time transform that one- dimension time series is decomposed to two- dimension time- time series, is used to protect the transformer. In addition, researchers have tried to make the differential relay more adaptive to the existing disturbance using a variable characteristic curve [25,26]. In Ref. [25], a protective method is implemented that divides the differential relay plane into three operating regions and two control regions with the corresponding weighting factors. A self-adaptive method is presented in Ref. [26] that adjusts itself according to the fault severity to avoid mal-operations.

In this paper, a new method based on Clark's transform and the modified hyperbolic S transform (MHST) is proposed for discrimination of internal faults from other abnormal conditions in power transformers such as inrush currents, external faults, over-excitation and ultra-saturation. By using Clark's transform and MHST, the researchers extracted important characteristics according to which different conditions could be distinguished and classified. In the proposed algorithm, the energy of different conditions extracted from the MHST matrix will

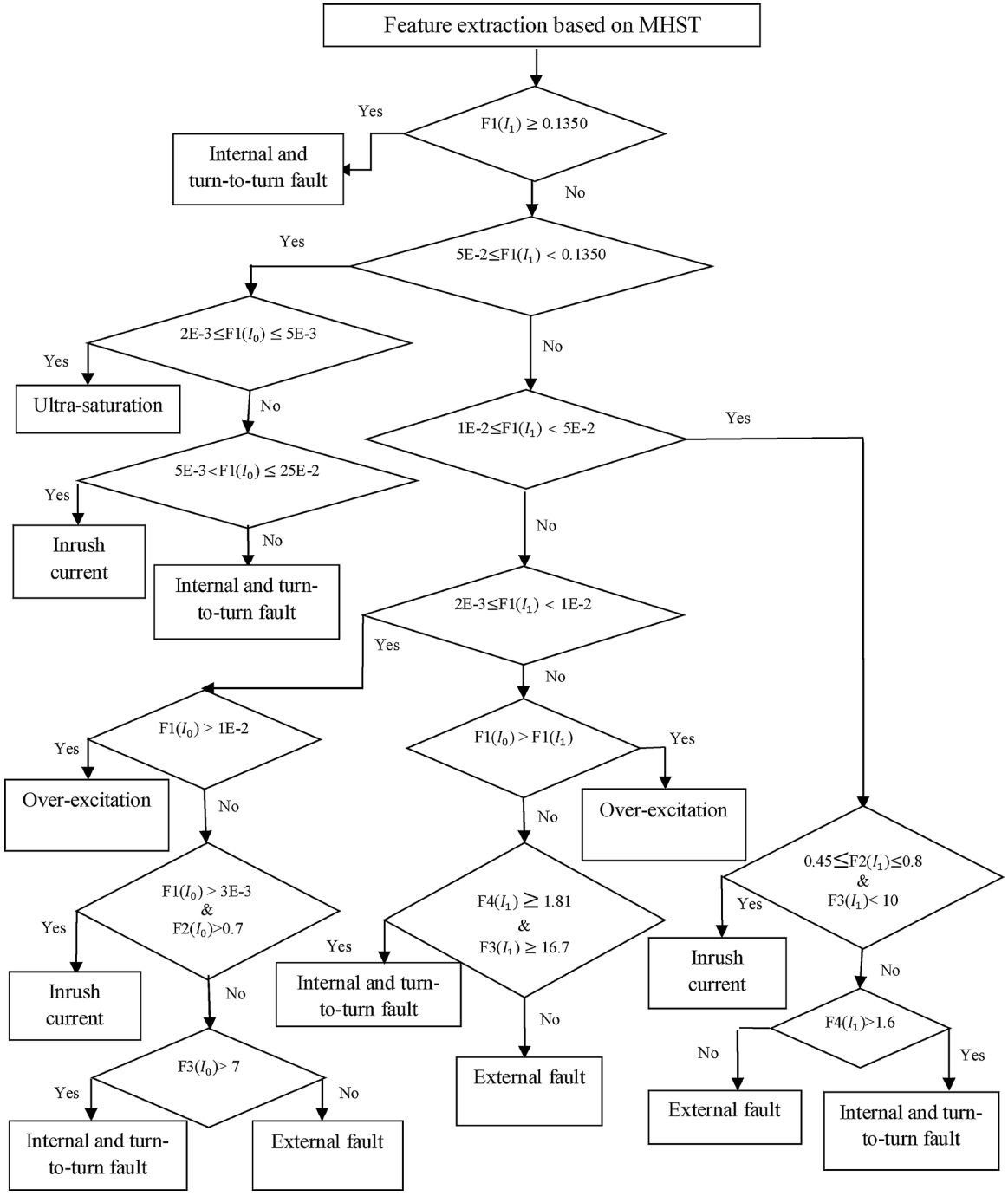

Fig. 2. The proposed algorithm for detecting fault and classification different conditions.

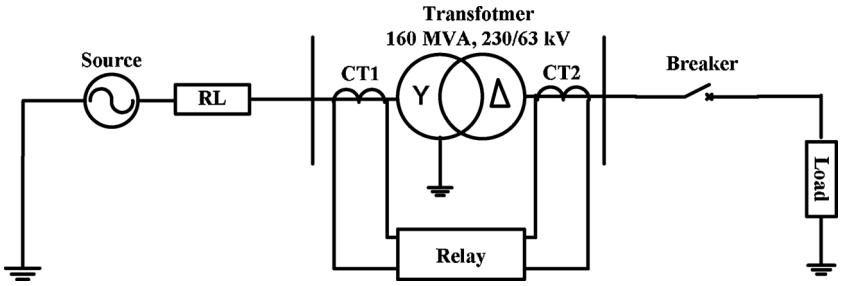

Fig. 3. Power system under study.

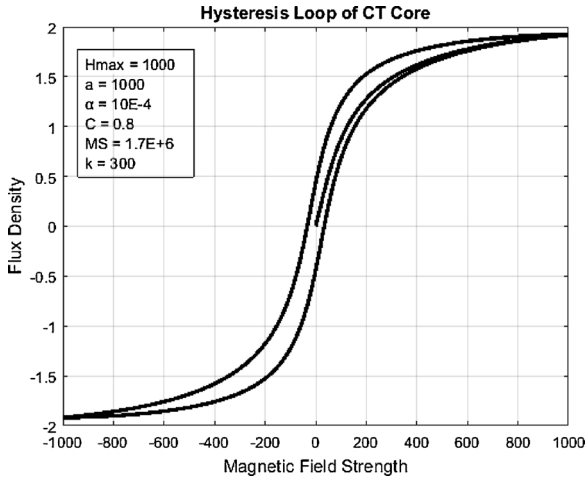

Fig. 4. Hysteresis loop of CT core.

be used as the main feature. This feature, due to the fact that the differential current amplitude differs in various simulations in a condition, divides the algorithm into five different parts. Other extracted features including variance index, standard deviation of the second harmonic component, and special criteria discriminate different conditions from each other in each part. The main advantages of this paper are following: (1) since all protection schemes require to consider every probable event, in this paper over-excitation and ultra-saturation conditions are investigated as two transient states, (2) one of the challenges that may cause mal-operation of protection relays is CT saturation, therefore, CT saturation in different conditions is investigated as another purpose of this paper, (3) In this paper the effect of noise on the proposed method in different conditions is considered, (4) The precision of classification corresponding to each part of the proposed algorithm is shown in this paper. The simulated results clearly show that the proposed technique can accurately discriminate between internal faults and other conditions in power systems.

2. Modified Hyperbolic S Transform

An S-transform is a frequency- time analysis that uses a Gaussian window to calculate S matrix [23]. An S-transform can be considered as a combination of Short time Fourier transform)STFT(and WT [23]. The expression of the ST is [27]:

$$S(\tau, f) = \int_{-\infty}^{+\infty} h(t)\omega(\tau - t)exp(-2\pi ift)dt \quad (1)$$

Where S is the S-transform of the time variable signal $h(t)$, τ is a parameter, which controls the position of Gaussian window on the time axis and f denotes the frequency.

The generalized S-transform provides more control on window function. Generalized S-transform is gained from S-transform [27] and substituting a generalized window with Gaussian window:

$$S(\tau, f, p) = \int_{-\infty}^{+\infty} h(t)\omega(\tau - t, f, p)exp(-2\pi ift)dt \quad (2)$$

where p denotes a set of parameters that govern the shape of the window. S-transform windows must satisfy Eq. (3):

$$\int_{-\infty}^{+\infty} \omega(\tau - t, f, p)d\tau = 1 \quad (3)$$

The Gaussian window has only one parameter, but the shape of the hyperbolic window is determined by a set of parameters [28]. Compared to S-transform, hyperbolic S-transform (HST) provides better resolution and transient analysis capabilities. Eq. (4) shows the HST

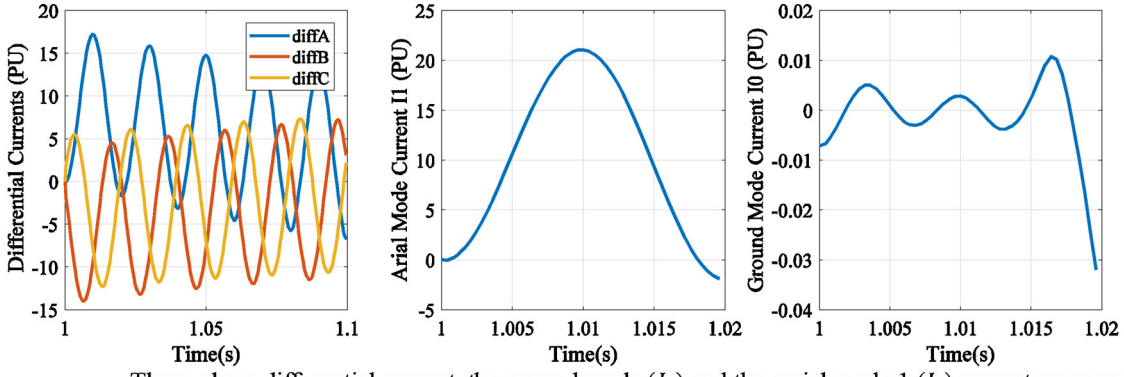

a- Three-phase differential current, the ground mode (I_0) and the aerial mode 1 (I_1) current components

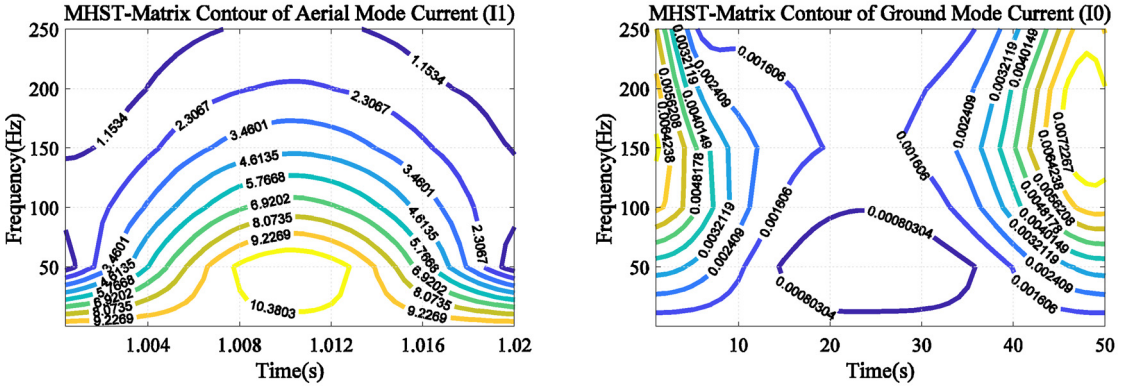

b- MHST contour of the ground mode (I_0) and the aerial mode 1 (I_1) current components

Fig. 5. Three-phase internal fault current.

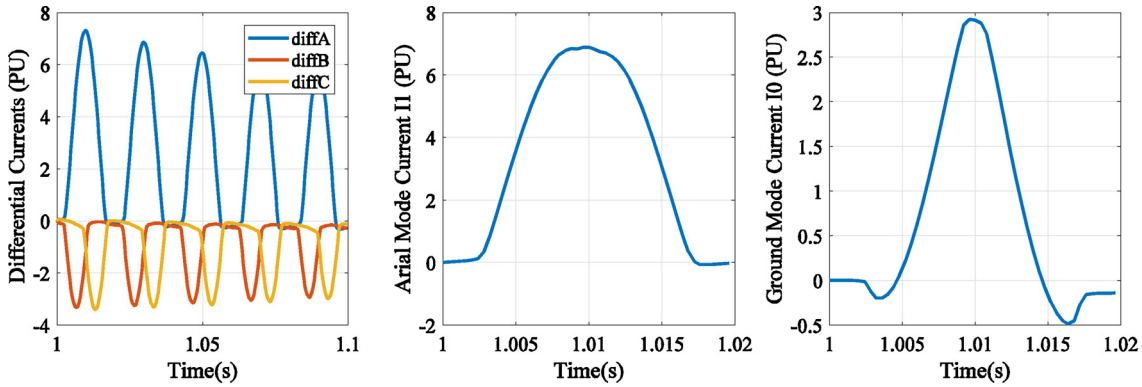

a- Three-phase differential current, the ground mode (I_0) and the aerial mode 1 (I_1) current components

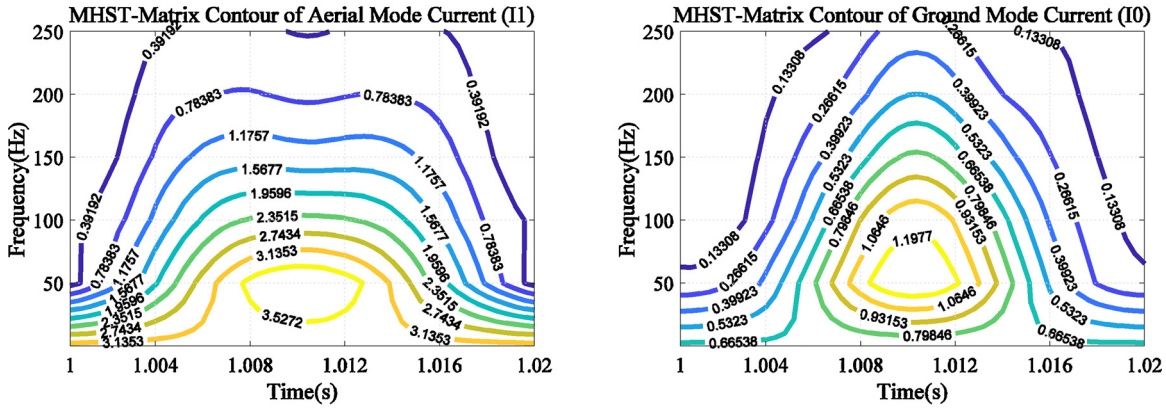

b- MHST contour of the ground mode (I_0) and the aerial mode 1 (I_1) current components

Fig. 6. Inrush current.

window:

$$\omega_{HY} = \frac{2|f|}{\sqrt{2\pi}(\gamma_a + \gamma_b)} \times exp[\frac{-f^2X^2}{2}] \tag{4}$$

Where

$$X(\tau - t, \{\gamma_a, \gamma_b, \lambda\}) = \frac{\gamma_a + \gamma_b}{2\gamma_a\gamma_b}(\tau - t - \xi) + \frac{\gamma_a - \gamma_b}{2\gamma_a\gamma_b}\sqrt{(\tau - t - \xi)^2 + \lambda^2} \tag{5}$$

In Eq. (5), X is a hyperbola in $(\tau - t)$ which depends upon a backward-taper parameter γ_a, a forward-taper parameter γ_b, and a positive curvature λ, which has units of time. In Eq. (5) $0 < \gamma_b < \gamma_a$ must be satisfied. The translation factor ξ is used to ensure that the peak of ω_{HY} occurs at $(\tau - t) = 0$ and this is defined in Eq. (6):

$$\xi = \sqrt{\frac{(\gamma_a - \gamma_b)^2\lambda^2}{4\gamma_a\gamma_b}} \tag{6}$$

In f = 0, ω_{HY} is asymmetrical, but as the frequency increases, ω_{HY} shape converges toward a symmetrical Gaussian window.

HST is more sensitive to noise. In order to solve this problem, MHST will be applied. The shape of MHST window is obtained according to Eq. (7):

$$\omega_{MHY} = \frac{2\sqrt{|fg|}}{\sqrt{2\pi}(\gamma_a + \gamma_b)} \times exp[\frac{-|fg|\ X^2}{2}] \tag{7}$$

Comparing Eqs. (4) and (7), it can be seen that the difference between the MHST and the HST is that the width of the MHST window is proportional to the square root of frequency. Besides, the MHST introduces a time-frequency regulation factor g that adjusts the time-frequency resolution.

The discrete version of the MHST is calculated in Eq. (8) [22]:

$$S[j, n] = \sum_{m=0}^{N-1} H[m + n]W_{MHY}(m, n)e^{\frac{i2\pi mj}{N}},\ n \neq 0 \tag{8}$$

$$S[j, 0] = \frac{1}{N}\sum_{m=0}^{N-1} h[m],\ n = 0 \tag{9}$$

Where N is the total number of samples and the indices n, m, and j are n = 0; 1; : : : ;N - 1; m = 0; 1; : : : ;N-1; and j = 0; 1; : : : ;N-1, respectively. H (m, n) denotes the frequency shifted discrete Fourier transform of the analyzed signal. W_{MHY} (m, n) is the Fourier transform of the hyperbolic window.

3. Proposed method

In this proposed method, as shown in Fig. 1, the secondary currents of the CTs on both sides of the power transformer are first measured. After normalizing the secondary currents of the CTs, eliminating the zero sequence of the secondary current of CT at the primary side and compensating the phase shift of the secondary current of CT at the secondary side, the three-phase differential currents are calculated. Then, the following steps are performed to discriminate internal faults from other conditions:

Step 1: In this algorithm, the activation current is initially calculated. The activation current of the differential protection is determined in Eq. (10) [5]:

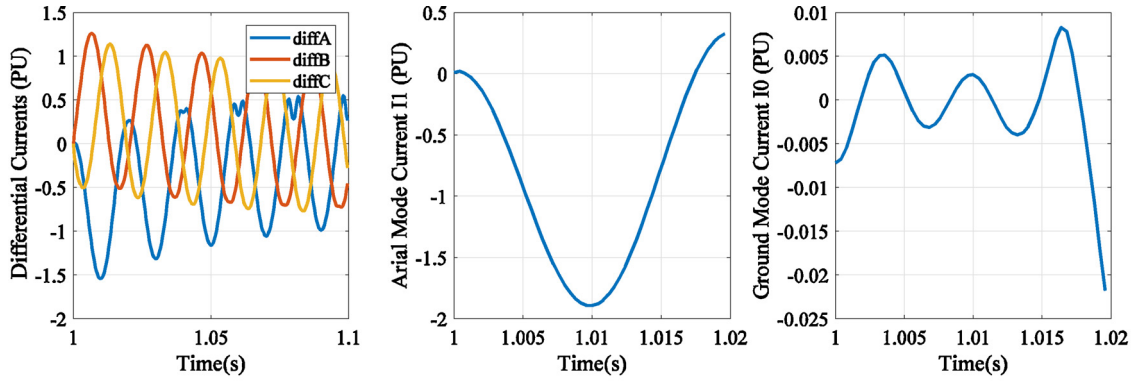

a- Three-phase differential current, the ground mode (I_0) and the aerial mode 1 (I_1) current components

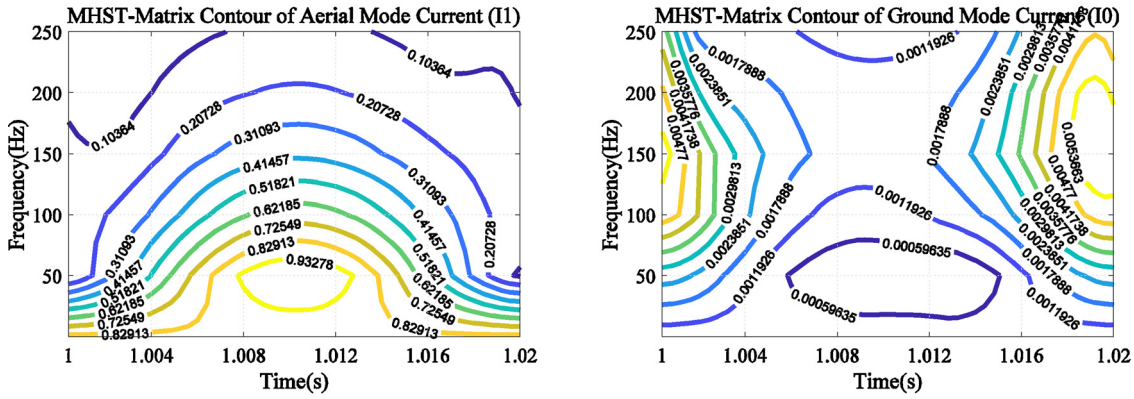

b- MHST contour of the ground mode (I_0) and the aerial mode 1 (I_1) current components

Fig. 7. Three-phase external fault current.

$$|I_{Diff,St}| = |k.\ I_{Res}| \tag{10}$$

Where k is the slope of the percentage differential relay characteristic and I_{Res} is the restraint current which calculated by Eq. (11):

$$I_{Res} = \frac{i_{1s} + i_{2s}}{2} \tag{11}$$

Where i_{1s} and i_{2s} are the secondary current CTs on the primary side and the secondary side of the power transformer, respectively.

According to Ref. [5], the threshold of $I_{Diff,St}$, is taken to be 0.25 pu. If all of the three-phase differential currents are less than this threshold, normal condition is detected. Otherwise, a transient condition is considered.

Step 2: Samples of currents will be collected for a cycle of fundamental frequency and given to Clark's transform. According to Eq. (12), the ground mode (I_0), aerial mode 1 (I_1) and aerial mode 2 (I_2) will be extracted from Clark's transform [18].

$$\begin{bmatrix} I_0 \\ I_1 \\ I_2 \end{bmatrix} = \frac{1}{\sqrt{3}} \begin{bmatrix} 1 & 1 & 1 \\ \sqrt{2} & -1/\sqrt{2} & -1/\sqrt{2} \\ 0 & \sqrt{3}/2 & -\sqrt{3}/2 \end{bmatrix} \begin{bmatrix} I_{da} \\ I_{db} \\ I_{dc} \end{bmatrix} \tag{12}$$

Step 3: The ground mode and aerial mode 1 will be considered as inputs of the MHST. Then the MHST is performed on one cycle of input data. For a data window of N samples, the MHST output is a $N/2 \times N$ matrix with complex elements. This matrix is called MHST-matrix that whose rows and columns relate to frequency and time domains, respectively [23]. Important information based on magnitude, phase and frequency can be obtained by means of this matrix. The magnitude contour equals the maximum value of the MHST matrix at a particular time (the maximum value in a specified column). The frequency contour is the maximum value of each frequency component in the differential current signal (the maximum value in each row).

3.1. Feature extraction

According to the information that can be obtained from the magnitude, phase and frequency of MHST matrix element, we can obtain various features for discriminating between the internal fault condition and other abnormal conditions. Based on the maximum and minimum magnitude, the average, the standard deviation, the variance corresponding to each row (related to frequency contour) and column (related to magnitude contour) in the MHST matrix, the area under frequency contour curve in different intervals, the MHST matrix energy, etc., different features will be obtained. Despite increasing the accuracy of the algorithm, using all of these features requires a large memory space. Increasing the computational burden of the algorithm will consequently reduce the speed of detection. Thus, to increase the speed of detection, the least important features should be selected. According to these two constraints, the balance between accuracy and speed must be considered in choosing the features.

The features gained from the MHST matrix are as follows:

- Energy of MHST contour first level (F1):

Energy of each MHST contour level is calculated according to Eq. (13):

$$Eng_{Li} = m_i \times T_i \tag{13}$$

Where m_i and T_i are the magnitude and the duration of the level of interest, respectively. Thus the energy of the MHST contour first level is:

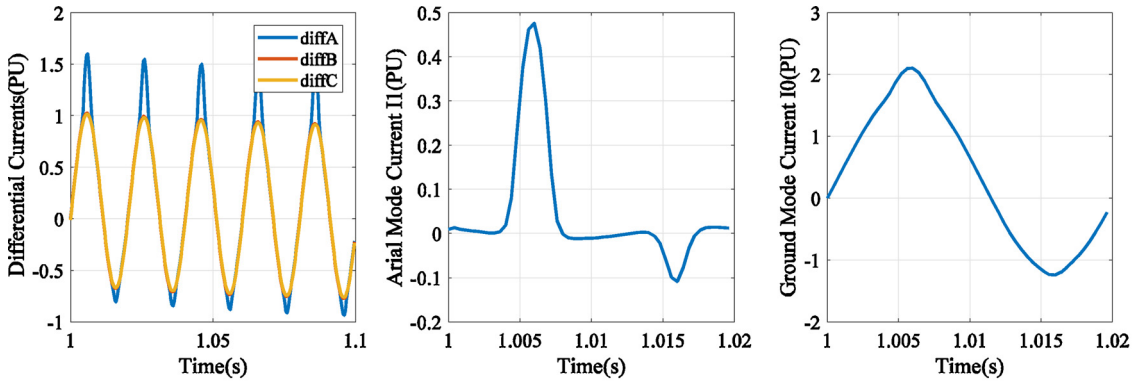

a- Three-phase differential current, the ground mode (I_0) and the aerial mode 1 (I_1) current components

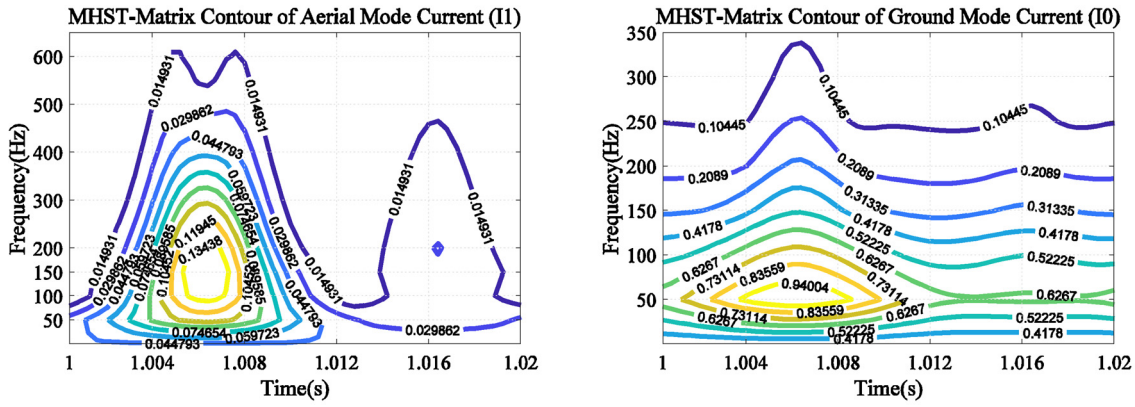

b- MHST contour of the ground mode (I_0) and the aerial mode 1 (I_1) current components

Fig. 8. Over-excitation current.

$$F1 = Eng_{L1} = m_1 \times T_1 \quad (14)$$

- Variance index (F2):

It is defined as:

$$F2 = V_2/V_1 \quad (15)$$

Where, V_1 is the variance of magnitudes of the second row of the MHST matrix (fundamental frequency) and V_2 is the variance of magnitudes of the third row of the MHST matrix (second harmonic frequency):

- Mixed energy-amplitude index (F3)

It is defined as:

$$F3 = |E_1\text{-}E_2| \times A_{\max}(f_1)/(A_{\max}(f_2) \times A_{0\max}) \quad (16)$$

Where, E_1 and E_2 are the first two biggest energy magnitudes of the MHST matrix that are obtained from Eq. (17):

$$E = abs(MHST)^2 \quad (17)$$

Where $A_{\max}$ (f_1), $A_{\max}$ (f_2) and $A_{0\max}$ are the maximum magnitude of the second row of the MHST matrix (fundamental frequency), the maximum magnitude of the third row of the MHST matrix (second harmonic) and the maximum magnitude of the first row of the MHST matrix (DC component), respectively, and f_1 and f_2 are the fundamental frequency and the second harmonic frequency, respectively.

- Phase standard deviation of second harmonic frequency (F4)

It is defined as:

$$F4 = Std(Ph\ (f_2)) \quad (18)$$

Where Std(Ph (f_2)) is the standard deviation of phases of the third row of the MHST matrix (second harmonic frequency).

These features are used for discriminating internal faults from other abnormal conditions.

3.2. Classification of different types of faults

After gaining meaningful features for the ground mode (I_0) and aerial mode 1 (I_1) of three phase differential currents in Fig. 2, these features are applied to the proposed algorithm. At each part, according to different conditions and the distinction among them, a specific range will be determined for each feature. At different parts, the various features are applied to the algorithm according to the ground mode and aerial mode 1.

An important feature that creates different parts in this algorithm is the energy of MHST contour first level for the aerial mode 1. The five main parts of the algorithm are created by determining different ranges for this feature. In different conditions that occur in the power system, the intensity and weakness of these conditions determine different energy amplitude. For example, Internal faults with low resistance produce high amplitude differential currents that lead to high energy generation. As it is specified in the algorithm in Fig. 2, the energy of MHST contour first level for the aerial mode 1 more than 0.1350 indicates that an internal fault has occurred. Different ranges of the energy of MHST contour first level for the aerial mode 1 constitute the other four parts of the algorithm.

To discriminate different conditions in each part, other features

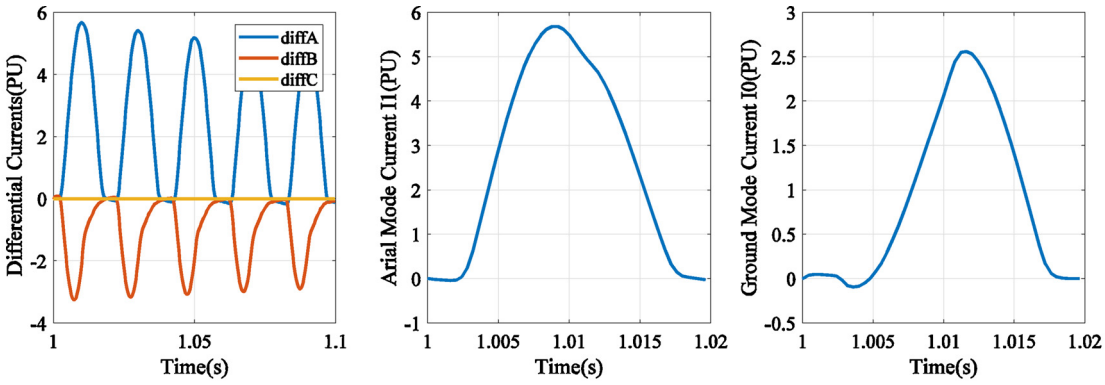

a- Three-phase differential current, the ground mode (I_0) and the aerial mode 1 (I_1) current components

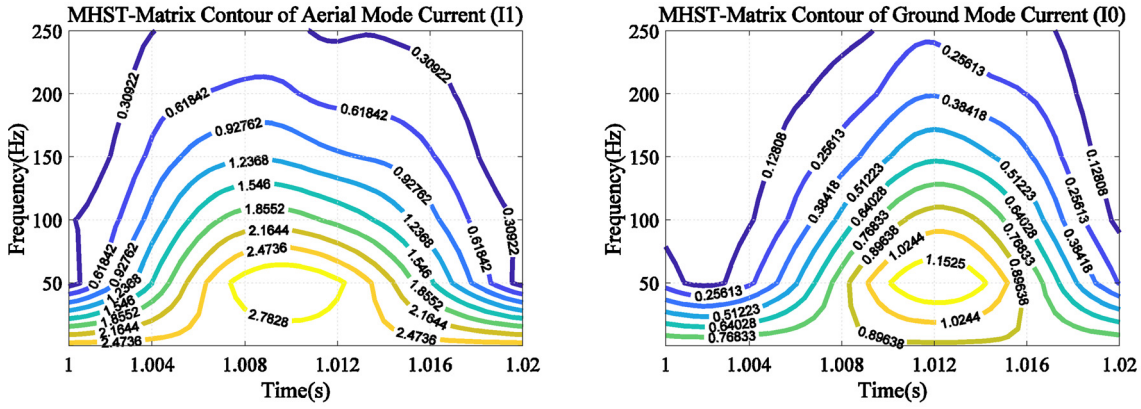

b- MHST contour of the ground mode (I_0) and the aerial mode 1 (I_1) current components

Fig. 9. Ultra-saturation current.

Table 1
Performance of the proposed method in the first part.

Condition	Correct detection	Incorrect detection	Accuracy %
Internal and turn-to-turn fault	86	–	100
Inrush current	–	–	–
External fault	–	–	–
Over-excitation	–	–	–
Ultra-saturation	–	–	–
Overall	86	–	100

Table 2
Performance of the proposed method in the second part.

Condition	Correct detection	Incorrect detection	Accuracy %
Internal and turn-to-turn fault	41	-	100
Inrush current	29	-	100
External fault	-	-	100
Over-excitation	-	-	-
Ultra-saturation	42	-	100
Overall	112	-	100

Table 3
Performance of the proposed method in the third part.

Condition	Correct detection	Incorrect detection	Accuracy %
Internal and turn-to-turn fault	48	-	100
Inrush current	40	-	100
External fault	10	–	100
Over-excitation	-	-	-
Ultra-saturation	-	-	-
Overall	98	–	100

Table 4
Performance of the proposed method in the fourth part.

Condition	Correct detection	Incorrect detection	Accuracy %
Internal and turn-to-turn fault	31	2	93.93
Inrush current	35	-	100
External fault	41	-	100
Over-excitation	3	-	100
Ultra-saturation	-	-	-
Overall	110	2	98.21

with various ranges are used. According to the energy of MHST contour first level for the aerial mode 1, the range of each feature in each part is different. The range for each feature in each part is defined according to different condition simulations.

While detecting some conditions such as an ultra-saturation condition needs only a few restrictions and is detectable in the second part of the algorithm, other conditions such as an internal and turn to turn fault, an external fault, an inrush current and an over-excitation are detected in several parts. This is because of the change in differential current amplitude while these conditions happen. A change in

Table 5
Performance of the proposed method in the fifth part.

Condition	Correct detection	Incorrect detection	Accuracy %
Internal and turn-to-turn fault	19	1	95
Inrush current	-	-	-
External fault	127	2	98.45
Over-excitation	73	-	100
Ultra-saturation	-	-	-
Overall	219	3	98.65

Table 6
Performance of the proposed method.

Condition	Correct detection	Incorrect detection	Accuracy %
Internal and turn-to-turn fault	225	3	98.68
Inrush current	104	-	100
External fault	178	2	98.88
Over-excitation	76	-	100
Ultra-saturation	42	-	100
Overall	625	5	99.21

amplitude in different conditions is influenced by source voltage angle changes, the residual flux changes, fault resistance change and the CT saturation.

4. Results

4.1. Power system simulation

The single line diagram for the power system under study is shown in Fig. 3. It consists of a three-phase 230 kV source connected to a three-phase, two-winding, power transformer 160 MVA, 230/63 kV. The transformer vector group is YNd11. The neutral of the high-voltage winding is grounded. The power transformer model and the corresponding CTs are developed in the PSCAD/EMTDC environment [29]. The parameters of the study system are given in the Appendix A.

Also, to represent CT real behavior in different conditions, a precise model was required. Thus, Jiles-Atherton model, explained in Ref. [30], was applied. The magnetization curve of CT core, i.e., the flux density versus magnetic field intensity, is illustrated in Fig. 4.

By performing the power system shown in Fig. 3 in PSCAD/EMTDC and running it in different conditions such as internal and turn-to-turn fault, external fault, inrush current, over-excitation and ultra-saturation, 630 cases of simulation are produced. The chosen sampling rate is 2.5 kHz at 50 Hz frequency, so a cycle contains 50 samples. In this paper, because of the capacity, one case study is shown in each condition.

To simulate different internal and external faults, the fault resistance is from 0 to 100 Ω and the switching angle is from 0 to 90° at intervals of 15°. Also, the effect of CT saturation on internal and external fault conditions is simulated in the worst possible case. In this condition, the remnant flux is considered 80% of the peak of linkages flux generated at rated voltage for a set of CTs at one side of the transformer (CTs of the other side are free from remnant flux). For turn-to-turn faults, simulations are carried out by changing the short circuited HV coil up to 45% of the winding and the LV coil up to 25% of the winding.

Different cases of inrush currents are simulated by changing the important parameters that affect it. These parameters include the remnant flux, the level of saturation flux and the switching angle at the instant of transformer energization. The remnant flux changes from ± 10% to ± 80% of peak of rated linkages flux and the switching angle changes from 0 to 90° at intervals of 15°. When transformers are connected in parallel, it is observed that the differential protection of the transformer that is in service issued a trip. The reason for this trip is sympathetic inrush current, which results from the inrush current of the transformer that is being energized. To simulate different cases of sympathetic inrush current, remnant flux of the incoming transformer changes from ± 10% to ± 80% of peak of rated linkages flux and the switching angle changes from 0 to 90° at intervals of 15°. The CT saturation effect is considered similar to the internal and external fault conditions.

The simulation of over-excitation conditions is performed by changing the amplitude of the voltage source and the switching angle. The amplitude of the voltage source changes from 1.15 to 1.35 pu and the switching angle changes from 0 to 90° at intervals of 15°.

To simulate different cases of ultra-saturation, the energization angle changes from 0 to 90° at interval of 15°. The remnant flux changes from ± 10% to ± 80% of peak of rated linkages flux in full-load condition of power transformer.

Figs. 5–9(a) show the three-phase differential current, the ground mode and the aerial mode 1 current components in the internal fault, inrush current, external fault, over-excitation and ultra-saturation conditions, respectively. According to Eq. (11), the ground mode and aerial mode 1 were calculated from Clark's transform of the three-phase differential current. The MHST contour curves of the ground mode and aerial mode 1 current components that provide comprehensive information of the desired signal-based frequency and time are shown in Figs. 5–9(b). These curves were obtained based on the MHST matrix. As shown in Figs. 4–8 (b), the curves are divided into 9 different levels. The level magnitudes for each condition were determined according to the maximum value of the MHST matrix. The highest values show the first level of the MHST contour and the lowest value shows the ninth level of the MHST contour. The difference between two consecutive levels is determined according to the number of desired levels, which is the same for both consecutive levels. In Eq. (13), where energy calculation of MHST contour level 1 is required, the first level magnitude in these curves was used. For example, according to Fig. 5(b) that shows the MHST contours of the ground mode and aerial mode 1 current components for a three-phase internal fault, the first level magnitudes were 10.3803 and 0.0064, respectively.

As shown in Figs. 5–9(b), the first level magnitude of the aerial mode 1 current component in the internal fault condition is the highest value, and in the over-excitation condition, it is the lowest value compared to other conditions. The first, second and third levels of the aerial mode 1 current component in the internal fault conditions are concentric around the fundamental and second harmonic. With respect to Figs. 5(b) and 7(b), the first level magnitude of the ground mode current component is negligible in both internal and external fault conditions. However, in the three conditions of inrush current, over-

Table 7
Performance of the proposed method in discriminating internal faults from other conditions.

Condition	Correct detection	Incorrect detection	Accuracy %
Internal and turn-to-turn fault	225	3	98.68
Other conditions	2	400	99.50
Overall	-	-	99.21

Table 8
The accuracy of the proposed method in discriminating different types of internal faults from other conditions.

Condition	Type of fault/abnormal condition	Simulation cases	Correct detection	Incorrect detection	Accuracy %
Internal faults	AG	36	34	2	94.44
	AB	36	36	–	100
	ABG	36	36	–	100
	ABC	36	35	1	97.22
	ABCG	36	36	–	100
	Turn to turn	48	48	–	100
External fault	AG	36	36	–	100
	AB	36	35	1	97.22
	ABG	36	35	1	97.22
	ABC	36	36	–	100
	ABCG	36	36	–	100
Inrush current	Changing the residual flux	22	22	–	100
	Changing the switching angle	82	82	–	100
Over-excitation	Changing the source amplitude	16	16	–	100
	Changing the switching angle	60	60	–	100
Ultra-saturation	Changing the residual flux	7	7	–	100
	Changing the switching angle	35	35	–	100

Table 9
Performance of the proposed method without Considering CT saturation.

Condition	Correct detection	Incorrect detection	Accuracy %
Internal and turn-to-turn fault	137	1	99.27
Inrush current	52	-	100
External fault	89	1	98.89
Overall	278	2	99.28

Table 10
Discrimination of internal fault from other conditions Considering CT saturation.

Condition	Correct detection	Incorrect detection	Accuracy %
Internal and turn-to-turn fault	88	2	97.78
Inrush current	52	-	100
External fault	89	1	98.89
Overall	229	3	98.71

Table 11
The effect of noise on the performance of the proposed algorithm.

Signal-to-noise ratio of 20 dB				Without noise
Condition	Correct detection	Incorrect detection	Accuracy %	Accuracy %
Internal and turn to turn fault	224	4	98.24	98.68
Inrush current	104	–	100	100
External fault	188	2	98.88	98.88
Over-excitation	76	–	100	100
Ultra-saturation	42	–	100	100
Overall	624	6	99.05	99.21

excitation and ultra-saturation, the first level magnitude of the ground mode (I_0) current component cannot be ignored. As seen in Figs. 7(b), 8(b) and 9(b), the first, second and third levels of the ground mode current component in the inrush current, over-excitation and ultra-saturation are concentric around the fundamental and second harmonic. In the case of over-excitation condition, unlike the other conditions, the first level magnitude of the ground mode current component is larger than the first level magnitude of the aerial mode 1 current component.

Tables 1–5 show the distinguished performance of the proposed method from the first part to the fifth part. Table 6 shows proper performance of the proposed method at detecting and classifying different conditions. The accuracy of the proposed method in discriminating an internal fault from other conditions is mentioned in Table 7. The proposed method's efficiency in different conditions is 99.18%. Therefore, it provides an effective discrimination between an internal fault and other conditions.

The proposed method's efficiency for all cases of internal faults, inrush currents, external faults, over-excitations and ultra-saturations are shown in Table 8. According to Table 8, the two cases of phase A-to-ground internal fault (AG) and a case of phase-to-phase internal fault (AB) in the internal fault conditions and a case of phase A-to-ground external fault (AG), a case of phase-to-phase-to-ground (ABG) external fault and a case of three-phase external fault (ABC) are detected incorrectly. However, the efficiency of the proposed method is 100% in other cases. As mentioned above, the CT saturation can cause mal-operation of the protection relay. So, the accuracy of the proposed method in different conditions, without/with the saturation of CTs, are given in Table 9 and 10, respectively. The accuracy of detecting different conditions without/with the saturation of CTs is 99.28% and 98.71%, respectively. The detection error rate for all conditions is 0.57%. These results indicate that CT saturation does not affect the proposed method.

To show the effect of noise on the proposed method, the signal-to-noise ratio of 20 dB was considered. This is the highest noise that can be added and reflects the practicability of the proposed method in actual power systems. As shown in Table 11, the noise is effective only in internal fault conditions, which is also negligible. Other conditions including external fault, inrush current, over-excitation and ultra-saturation are not affected by the noise.

Also, the effect of different vector groups on the proposed method is been investigated. In this paper, a three-phase transformer YNd11 is been used. Comparison of the results of the proposed method for a three-phase transformer with YNd1 and YNd5 vector groups with a three-phase transformer YNd11 vector group, is shown in the Table 12. According to the results presented, it can be seen that the performance

Table 12
Comparing accuracy of classification and detection in different vector groups.

Vector group	YNd1	YNd5	YNd11
Internal and turn-to-turn fault	97.37%	98.24%`	98.68%
Inrush current	100%	100%	100%
External fault	98.33%	98.88%	98.88%
Over-excitation	100%	100%	100%
Ultra-saturation	100%	100%	100%
Overall	98/57%	99.04%	99.21%

Table 13
Comparing accuracy of classification and detection in different methods.

Condition	ANN + PSO [31]	WT [32]	HST [22]	KNN + GA [8]	HST + PNN [23]	Proposed method
Internal and turn-to-turn fault	100%	100%	98.24%`	100%	99.12%	98.68%
Inrush current	100%	100%	99.04%	99.04%	99.04%	100%
External fault	–	100%	97.22%	–	98.33%	98.88%
Over-excitation	–	–	–	97.36%	98.68%	100%
Ultra-saturation	–	–	–	–	–	100%
Overall	100%	100%	98.05%	99.26%	98.81%	99.21%

Table 14
Comparing accuracy of classification and detection in different methods with noise.

Condition	ANN + PSO [31]	WT [32]	HST [22]	KNN + GA [8]	HST + PNN [23]	Proposed method
Internal and turn-to-turn fault	–	–	97.80%	–	98.68%	98.24%
Inrush current	–	–	98.08%	–	98.08%	100%
External fault	–	–	97.22%	–	97.22%	98.18%
Over-excitation	–	–	–	–	96.05%	100%
Ultra-saturation	–	–	–	–	–	100%
Overall	–	–	97.65%	–	97.79%	99.05%

of the proposed method in different vector groups is not very different.

Comparisons of the results of various methods in conditions with noise and without noise are shown in Tables (13) and (14), respectively. In Ref. [31], the probabilistic neural network (PNN) is proposed to discriminate between transformer internal fault and inrush current condition. The particle swarm optimization is applied to obtain an optimal smoothing factor of PNN. The proper operation in distinguishing internal fault conditions from the current is the advantage of this method. The disadvantage of this study is not to consider the external faults, over-excitation and ultra-saturation conditions and the effect of the noise on the proposed method. In Ref. [32], the wavelet transform is used to distinguish and classify different conditions. Despite the proper performance in internal fault conditions as well as in external fault and inrush current, over-excitation and ultra-saturation conditions, as two other transient states, are not investigated. The accuracy of detecting the internal fault, the external fault and the inrush current in [22] (HST) is 98.2%, 97.22% and 99.04%, respectively, and when the 20-dB noise is considered, the accuracy of internal fault detection, external fault and inrush current is 97.9%, 97.22% and 98.08%, respectively. In Ref. [22], despite the fact that different conditions are considered with noise, the study is not considered ultra-saturation and over-excitation. In Ref. [8], where a hybrid intelligent method is used, the accuracy rate of detecting internal fault, inrush current, and over-excitation is 100%, 99.04%, and 97.36%, respectively. In addition to disregarding the noise conditions, it does not investigate external fault and ultra-saturation conditions either. In Ref. [23], where HST is used with a probabilistic neural network, the accuracy of internal fault, external fault, inrush current and over-excitation detection is 99.9%, 98.33%, 99.04% and 98/68% respectively, And when a 20-dB noise is considered, the accuracy of internal fault, external fault, inrush current and over-excitation detection is 98.68%, 97.22%, 98.08% and 96/05%, respectively. In Ref. [23], despite the proper accuracy and the inclusion of more transient conditions, the ultra-saturation condition is not studied.

In the worst case, 12 ms must be passed from the inception of fault to detect internal fault conditions. Moreover, 4 ms is needed for signal processing and decision stages according to the flowchart of the proposed fault detection scheme. Therefore, the total time taken by the proposed protection scheme is approximately 16 ms from the inception of fault.

5. Conclusion

This paper presents a new method based on Clark's transform and MHST to discriminate internal and turn-to-turn faults from other conditions. Over-excitation and ultra-saturation are two other conditions that must not cause the relay to operate. In this paper, both the over-excitation and the ultra-saturation conditions along with other conditions are considered for the first time. MHST is used as a time-frequency analyzer of non-stationary differential current signals and provides a superior performance compared to the S-transform. Thus, according to the MHST matrix, a set of meaningful features will be extracted. Unlike the algorithms based on ANN, this method does not need training or testing the extracted features. The detection is done by a few simple comparisons.

In the CT saturation condition which can lead to relay mal-operation, the proposed method shows desirable performance. Moreover, the simulation results show that unlike wavelet-based techniques, the proposed method is immune to noise. The accuracy and speed of the detection of different conditions show the proper operation of the proposed method.

Declaration of Competing Interest

The authors declare that they have no known competing financial interests or personal relationships that could have appeared to influence the work reported in this paper.

Appendix A

Source

$\boldsymbol{V_S} = 230\,\mathbf{kV}$, $\boldsymbol{Z_S}= 1 + j1.57\ \mathbf{\Omega}$

Power transformer

160 **MVA**, 230/63 **Kv**, 50 Hz, YND11, Leakage Reactance = 0.1 **pu**, Magnetizing Current = 1%

Current transformer

Primary side

CT Ratio: 600:1, $\boldsymbol{R_s} = 4.3\ \mathbf{\Omega}$, $\boldsymbol{L_s} = 1E\text{-}4\ \mathbf{H}$, $A = 32.9E\text{-}4\,\mathbf{m}^2$,

L = 0.848 **m**

Secondary side

CT Ratio: 2000:1, $\boldsymbol{R_s}$ = 7.77 **Ω**, $\boldsymbol{L_s}$ = 1E-5 **H**, A = 10.36E-4 $\mathbf{m}^2$, L = 0.548 **m**

References

[1] J.L. Blackburn, T.J. Domin, Protective Relaying: Principles and Applications, Third edition, Taylor & Francis, 2006.
[2] ABB, Protection Application Handbook, (1999).
[3] S.K. Murugan, S.P. Simon, P.S.R. Nayak, K. Sundareswaran, N.P. Padhy, Power transformer protection using chirplet transform, IET Gener. Transm. Distrib. 10 (10) (2016) 2520–2530.
[4] M.Y. Asrami, M.T. Gorjikolaie, S.M. Razavi, S.A. Gholamian, A novel intelligent protection system for power transformers considering possible electrical faults, inrush current, CT saturation and over-excitation, Electr. Power Energy Syst. 64 (2015) 1129–1140.
[5] S. Horowitz, A. Phadke, Power System Relaying, Research Studies Press, Taunton, Somerset, 1992.
[6] H. Zhang, P. Liu, O.P. Malik, A new scheme for inrush identification in transformer protection, Electr. Power Syst. Res. 63 (2) (2002) 81–86.
[7] D. Guillen, H. Esponda, E. Vazquez, G. Idarraga-Ospina, Algorithm for transformer differential protection based on wavelet correlation modes, IET Gener. Transm. Distrib. 10 (12) (2016) 2871–2879.
[8] P.B. Thote, M.B. Daigavane, P.M. Daigavane, S.P. Gawande, An intelligent hybrid approach using KNN-GA to enhance the performance of digital protection transformer scheme, Can. J. Electr. Comput. Eng. 40 (3) (2017) 151–161.
[9] T. Zheng, T. Huang, Y. Ma, Z. Zhang, L. Liu, Histogram-based method to avoid maloperation of transformer differential protection due to current-transformer saturation under external faults, IEEE Trans. Power Deliv. 33 (2) (2018) 610–619.
[10] H. Dashti, M. Davarpanah, M. Sanaye-Pasand, H. Lesani, Discriminating transformer large inrush currents from fault currents, Electr. Power Energy Syst. 75 (2016) 74–82.
[11] A. Rahmati, M. Sanaye-Pasand, Protection of power transformer using multi criteria decision-making, Int. J. Electr. Power Energy Syst. 68 (2015) 294–303.
[12] S. Hasheminejad, S. Esmaeili, Transient actions analysis of power transformers-based on S-transform and hidden Markov model, Int. Trans. Electr. Energy Syst. 24 (2014) 826–841.
[13] T. Zheng, J. Gu, S.F. Huang, F. Guo, V. Terzija, A new algorithm to avoid maloperation of transformer differential protection in substations with an inner bridge connection, IEEE Trans. Power Deliv. 27 (3) (2012) 1178–1185.
[14] K.L. Butler-Purry, M. Bagriyanik, Characterization of transients in transformers using discrete wavelet transforms, IEEE Trans. Power Syst. 18 (2) (2003) 648–654.
[15] A. Aktabi, M.A. Rahman, A.M. Razali, An experimental implementation of the dq-axis wavelet packet transform hybrid technique for three-phase power transformer protection, IEEE Trans. Ind. Appl. 50 (4) (2014) 2919–2927.
[16] A.M. Shah, B.R. Bhalja, Discrimination between internal faults and other disturbances in transformer using the support vector machine-based protection scheme, IEEE Trans. Power Deliv. 28 (3) (2013) 1508–1515.
[17] M. Rasoulpoor, M. Banejad, A correlation based method for discrimination between inrush and short circuit currents in differential protection of power transformer using discrete wavelet transform: theory, simulation and experimental validation, Int. J. Electr. Power Energy Syst. 51 (2013) 168–177.
[18] B. Noshad, M. Razaz, S.G. Seifossadat, A new algorithm based on Clarke's transform and discrete wavelet transform for the differential protection of three-phase power transformers considering the ultra-saturation phenomenon, Electr. Power Syst. Res. 110 (May) (2014) 9–24.
[19] R. Kumar, B. Singh, D.T. Shahani, A. Chandra, K. Al-Haddad, Recognition of power-quality disturbances using S-transform-based ANN classifier and rule-based decision tree, IEEE Trans. Ind. Appl. 51 (1) (2015) 2919–2927.
[20] M. Biswal, P.K. Dash, Measurement and classification of simultaneous power signal patterns with an S-transform variant and Fuzzy decision tree, IEEE Trans. Ind. Appl. 9 (4) (2013) 1819–1827.
[21] Z. Moravej, A.A. Abdoos, M. Sanaye-Pasand, Power transformer protection using improved S-transform, Electr. Power Comp. Syst. 39 (11) (2011) 1151–1174.
[22] A. Ashrafian, M. Rostami, G.B. Gharehpetian, Hyperbolic S-transformbased method for classification of external faults, incipient faults, inrush currents and internal faults in power transformers, IET Gener. Transm. Distrib. 6 (10) (2012) 940–950.
[23] Z. Moravej, A.A. Abdoos, M. Sanaye-Pasand, Power transformer protection scheme based on time-frequency analysis, Int. Trans. Electr. Energy Syst. 23 (4) (2013) 473–493.
[24] A. Ashrafian, B. Vahidi, M. Mirsalim, Time–time-transform application to fault diagnosis of power transformers, IET Gener. Transm. Distrib. 8 (6) (2014) 1156–1167.
[25] H. Dashti, M. Sanaye-Pasand, Power transformer protection using a multiregion adaptive differential relay, IEEE Trans. Power Deliv. 29 (2) (2014) 777–785.
[26] W. Zhang, Q. Tan, S. Miao, L. Zhou, P. Liu, Self-adaptive transformer differential protection, IET Gener. Transm. Distrib. 7 (1) (2013).
[27] R.G. Stockwell, L. Mansinha, R. Lowe, Localization of the complex spectrum: the Stransform, IEEE Trans. Signal Process. 44 (1996) 998–1001.
[28] C.R. Pinnegar, L. Mansinha, The S-transform with windows of arbitrary and varying shape, Geophysics 68 (January (1)) (2003) 381–385.
[29] P. Wilson, Applications of PSCAD/EMTDC, Manitoba HVDC Reseach Center, Winnipeg, MB, Canada, 2007.
[30] D.C. Jiles, J.B. Thoelke, M. Devine, Numerical determination of hysteresis parameters using the theory of ferromagnetic hysteresis, IEEE Trans. Magn. 28 (1) (1992) 27–35.
[31] M. Tripathy, R.P. Maheshwari, H.K. Verma, Power transformer differential protection based on optimal probabilistic neural network, IEEE Trans. Power Deliv. 25 (January (1)) (2010) 102–112.
[32] R.P. Medeiros, F.B. Costa, A wavelet-based transformer differential protection with differential current transformer saturation and cross country fault detection, IEEE Trans. Power Deliv. 33 (2) (2018) 789–799.